Second harmonic generation in reverse proton exchanged Lithium Niobate waveguides

Annarita Di Lallo, Alfonso Cino[*]**, Claudio Conti and Gaetano Assanto**

National Institute for the Physics of Matter INFM-RM3 &
Department of Electronic Engineering, Terza University of Rome
Via della Vasca Navale 84, 00146 Rome - ITALY
Assanto@ele.uniroma3.it

* Permanent address: Center for Electronics Research in Sicily (CRES), Monreale (PA), Italy.

Abstract: We investigate efficient second harmonic generation in reverse proton exchanged Lithium Niobate waveguides. In z-cut crystals, the resulting buried and surface guides support TM and TE polarizations, respectively, and are coupled through the d_{31} nonlinear element. Numerically estimated conversion efficiencies in planar structures operating at 1.32μm reach 90% in 2cm or a normalized 14% μm/W cm.
©2001 Optical Society of America

References and links

1. See, for example, A. M. Prokhorov, U. S. Kuz'minov, O. A. Khachaturyan, *Ferroelectric Thin Film Waveguides in Integrated Optics and Optoelectronics*, Cambridge International Science Publ., 1996
2. X. F. Cao, R. V. Ramaswamy, and R. Srivastava, "Characterization of annealed proton exchanged LiNbO$_3$ waveguides for nonlinear frequency conversion," J. Lightw. Technol. **10**, 1302-1315 (1992)
3. J. L. Jackel, and J. J. Johnson, "Reverse exchange method for burying proton exchanged waveguides," Electron. Lett. **27**, 1360-1361 (1991)
4. J. Olivares, J. M. Cabrera, "Modification of proton exchanged LiNbO$_3$ layers for guiding modes with ordinary polarization," Fiber Integ. Optics **12**, 277-285 (1993)
5. J. Olivares, J. M. Cabrera, "Guided modes with ordinary refractive index in proton exchanged LiNbO$_3$ waveguides," Appl. Phys. Lett. **62**, 2468-2470 (1993)
6. P. Baldi, M. De Micheli, K. El Hadi, A. C. Cino, P. Aschieri, and D. B. Ostrowsky, "Proton exchanged waveguides in LiNbO$_3$ and LiTaO$_3$ for integrated lasers and nonlinear frequency converters," Opt. Eng. **37**, 1193-1202 (1998).
7. K. El Hadi, P. Baldi, M. P. De Micheli, D. B. Ostrowsky, Y. N. Korkishko, V. A. Fedorov, and A. V. Kondrat'ev, "Ordinary and extraordinary waveguides realized by reverse proton exchange on LiTaO$_3$," Opt. Commun. **140**, 23-26 (1997)
8. Y. N. Korkishko, V. A. Fedorov, T. M. Morozova, F. Caccavale, F. Gonella, and F. Segato, "Reverse proton exchange for buried waveguides in LiNbO$_3$," J. Opt. Soc. Am. A **15**, 1838-1842 (1998)
9. J. Rams, J. Olivares, and J. M. Cabrera, "SHG-capabilities of reverse PE-LiNbO$_3$ waveguides," Electron. Lett. **33**, 322-323 (1997)
10. A. W. Snyder and J. D. Love, *Optical Waveguide Theory* (Chapman & Hall, London, 1983)
11. G. R. Hadley, "Transparent boundary condition for the beam propagation method," IEEE J. Quantum Electron. **28**, 363-370 (1992)
12. G. J. Edwards and M. Lawrence, "A temperature dependent dispersion for congruently grown lithium niobate," Opt. & Quantum Electron. **16**, 373-374 (1984)
13. K. Chikuma and S. Umegaki, "Characteristics of optical second-harmonic generation due to Cerenkov-radiation-type phase matching," J. Opt. Soc. Am. B **7**, 768-775 (1990)
14. M. De Micheli, "Second harmonic generation in Cerenkov configuration" in *Guided Wave Nonlinear Optics*, D. B. Ostrowsky and R. Reinisch eds. (Kluwer Acad. Publishers., Dordrecht, NL 1992)
15. G. Arvidsson and F. Laurell, "Nonlinear optical wavelength conversion in Ti:LiNbO$_3$ waveguides," Thin Solid Films **136**, 29-36 (1986)

16. N. A. Sanford and J. M. Connors, "Optimization of the Cerenkov sum-frequency generation in proton-exchanged Mg:LiNbO$_3$ channel waveguides," J. Appl. Phys. **65**, 1430-1437 (1989)
17. G. Tohmon, J. Ohya, K. Yamamoto, and T. Taniuchi, "Generation of ultraviolet picosecond pulses by frequency-doubling of laser diode in proton-exchanged MgO:LiNbO$_3$ waveguide," IEEE Phot. Techn. Lett. **2**, 629-631 (1990)
18. W. Sohler and H. Suche, "Second-harmonic generation in Ti-diffused LiNbO$_3$ waveguides with 25% conversion efficiency," Appl. Phys. Lett. **33**, 518-520 (1978)

1. Introduction

Among man-made crystals for electro-optics and nonlinear photonics, Lithium Niobate (LN) is probably the most investigated and employed. It allows efficient phase and amplitude modulation and parametric generation in guided-wave configurations [1]. Several specific technologies have been mastered in order to fabricate LN planar integrated devices, from Titanium in-diffusion to ion-exchange to e-beam implantation, etc. Among them, proton exchange (PE) combines the advantages of a low-temperature process with a substantial surface index increase and a reduced photorefractive sensitivity [2]. Despite their high quality, even with additional improvements such as thermal annealing, soft exchange in diluted solutions, sealed ampoule method, etc., the asymmetric profile of PE waveguides is an obstacle to efficient coupling to/from silica fibers. In order to improve such coupling between waveguide and LP$_{01}$ fiber modes, Reverse PE (RPE) was recently introduced to obtain buried and more symmetric channel waveguides.[3-8]

RPE is a two-step process: a first, deeply penetrating $H^+ \rightarrow Li^+$ exchange followed by a second, weaker $Li^+ \rightarrow H^+$ exchange. Such technique allows to form two superimposed waveguides with graded index profiles, each of them able to confine one of the principal (orthogonal) polarizations. For a z-cut crystal, for instance, an ordinary ray can be confined as a TE guided mode, while an extraordinary ray becomes a TM eigenfields. As sketched in Fig. 1, TE and TM waves can then propagate and carry power along y at different depths, corresponding to the two (ordinary and extraordinary) refractive distributions.
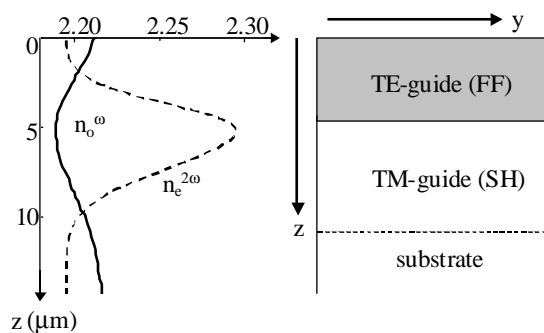

Fig. 1. RPE geometry with graphs of ordinary and extraordinary index distributions in z-cut LN.

These superimposed waveguides can be coupled by a nonlinear interaction involving a non-diagonal element, i. e., thru a polarization field orthogonally polarized with respect to the input electric wave. This is the typical configuration of a Type I phase-matched process of Second-Harmonic Generation (SH-G), whereby the harmonic is orthogonal to the fundamental frequency (FF) field. Furthermore, this is the standard SHG taking place in uniform birefringent phase-matched LN crystals thru the d$_{31}$ element of the quadratic susceptibility, the largest non-diagonal. It is worth underlining that the double exchange tends to recover the quadratic nonlinear response of the surface layer, contrary to single-step PE [9]. Therefore,

using mode coupling between fundamental and second harmonics in the surface and buried guides of an RPE geometry, respectively, one expects the generation of a TM frequency-doubled field by injecting a TE FF wave in the upper waveguide.

In this Paper we investigate numerically SHG in RPE planar waveguides in z-cut propagation-homogeneous (non-periodically-poled) LN, and demonstrate that large conversion efficiencies can be obtained even in those cases when much higher or lower temperatures would be required in the absence of Quasi-Phase-Matching, with good fabrication tolerances and physical separation of the harmonic field distributions at the output.

2. Models

Let us consider a z-cut y-propagating LN crystal. The pertinent non-diagonal elements of the second-order tensor **d** will couple z and x components of the electric-field. An FF wave propagating in the surface waveguide as a TE mode will radiate a cross-polarized SH field into the buried guide, supporting TM eigenwaves (see the extraordinary -dashed- index profile in Fig. 1). We will assume the upper guide is single-moded at the FF wavelength, whereas the deep guide is multimodal at the SH, the most common situation in a practical realization:

$$E_{TE}^{\omega}(z,y) = A(y)f_{\omega}(z)e^{-ik_0 N_{\omega} y} \quad , \quad E_{TM}^{2\omega}(z,y) = \sum_{\nu} B_{\nu}(y) f_{2\omega}^{\nu}(z) e^{-i2k_0 N_{2\omega}^{\nu} y} \qquad (1)$$

with k_0 the vacuum wave-number at FF and N the effective index. The generation will then take place through the interaction between the fundamental FF mode and high-order SH modes, whenever phase-matching is accomplished with an appreciable overlap integral $I = \int (f_{2\omega}^{\nu})^* f_{\omega}^2 dz$, as prescribed by coupled-mode theory (CMT) [10].

In a structure of finite length, however, the interaction is better described by a system of partial differential equations taking into account the details of the geometry and the overall field distributions undergoing nonlinear propagation and energy exchange. For the superposition of cross-polarized (FF and SH) harmonics propagating along y in a z-cut LN crystal, using Maxwell equations in the usual approximation of weak guidance and keeping the second derivatives with respect to y, we get:

$$\frac{\partial^2 E_{TE}^{\omega}}{\partial y^2} + \frac{\partial^2 E_{TE}^{\omega}}{\partial z^2} + k_0^2 (n_o^{\omega}(z))^2 E_{TE}^{\omega} + 2k_0^2 d_{15} \, E_{TM}^{2\omega}(E_{TE}^{\omega})^* = 0$$

$$\frac{\partial^2 E_{TM}^{2\omega}}{\partial y^2} + \frac{(n_{es}^{2\omega})^2}{(n_{os}^{2\omega})^2} \frac{\partial^2 E_{TM}^{2\omega}}{\partial z^2} + 4k_0^2 (n_e^{2\omega}(z))^2 E_{TM}^{2\omega} + 4k_0^2 d_{31} \, (E_{TE}^{\omega})^2 = 0$$

$$(2)$$

with n_o^{ω} and $n_e^{2\omega}$ the ordinary and extraordinary graded index distributions at FF and SH, respectively, $n_{os}^{2\omega}$ and $n_{es}^{2\omega}$ the bulk (i. e., substrate) ordinary and extraordinary indices at SH, $d_{15}=d_{31}$ the relevant nonlinear coefficients when Kleinmann symmetry holds. The set (2) can be integrated using the Enhanced Finite Difference Beam Propagation Method (EFDBPM) with transmitting boundary conditions [11].

To evaluate the nonlinear response in a realistic case, we considered typical index profiles for planar RPE waveguides, as prepared and reported by Korkishko *et al.* in z-cut LiNbO$_3$ [8]. The samples were first PE-treated for 14h in an Ammonium Di-Hydrophospate melt at 220°C, then they were thermally annealed for 110h at 330°C; finally, they were RPE-processed in a LiNO$_3$ melt for 100h at 300°C. For a wavelength $\lambda = 2\pi c/\omega = 1.32\mu m$ such that the top guide supports one mode at FF, i. e., the index distributions can be expressed as:

$$n_{o,e}^{q\omega}(z) = n_{os,es}^{q\omega} + \Delta n_{o,e}^{q\omega} \exp\left(-\frac{z-z_0}{\sigma_{oi,ei}}\right)^2 \tag{3}$$

with q=1 (2) for the FF (SH), **i=1 (2)** $\forall$ $z<z_0$ ($\forall$ $z>z_0$), $z_0=6\mu m$, $\sigma_{o1}=4\mu m$, $\sigma_{o2}=5\mu m$, $\sigma_{e1}=2\mu m$, $\sigma_{e2}=3\mu m$, $\Delta n_o^\omega = -0.028$ and $\Delta n_e^{2\omega} = 0.1$.

    For the profiles (3) and q=1, we calculated the FF eigenmodes with a Finite Difference Method (FDM). Then, we integrated eqns. (2) launching in the upper guide suitable FF field distributions and studying the y-evolutions of FF and SH waves. In our simulations we employed either an LP01-like (x-invariant) Gaussian beam with a symmetric distribution $u_1(z) = \exp[-(z-z_1)^2/\sigma^2]$ optimally centered at $z_1=3\mu m$ with $\sigma=0.83z_1$; or the zeroth-order TE eigenmode as derived numerically by FDM. Integrating the SH field and its intensity over the output transverse (z) section at a distance L from the input, we evaluated SHG conversion efficiencies (per unit wavefront along x) for various excitation levels, temperatures and device lengths.

3. Results and discussion

Let us first compare the outcomes from standard CMT and EFDBPM with eqns. (2). For a 1cm-long sample at 25°C, it is apparent from Fig. 2 that the computed conversion efficiency with the two approaches (using a Gaussian excitation for the EFDBPM) is markedly different. Examining in more detail the case of a Gaussian excitation, mapping FF and SH intensities
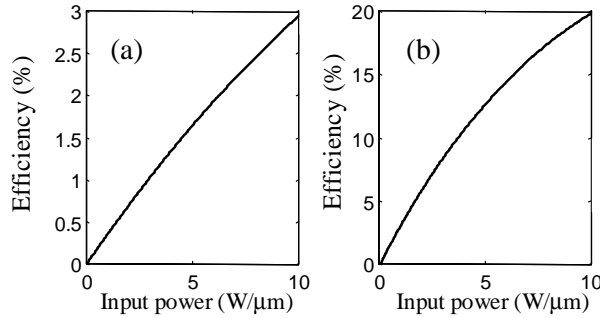

Fig. 2. Computed SHG conversion efficiency versus input power for a 1cm sample at 25°C. (a) CMT and (b) EFDBPM results in case of Gaussian excitation.

versus propagation and depth, we see in Fig. 3 that, for a 10W/µm input power into an RPE waveguide of length L=2cm, nearly 80% of the input beam couples to the TE_0 mode of the upper waveguide, with the remaining 20% exciting a leaky or quasi-mode, as apparent from the lobes visible across the depth coordinate z (Fig. 3a). The parametric nonlinearity generates a TM polarized SH field which, confined in the buried waveguide, grows with propagation. The competition between the two excited modes at FF, however, limits the overall up-conversion efficiency. This insight is supported by Fig. 4, showing the effective index versus modal number at SH at 25°C. The 10th mode is close to phase match the fundamental FF mode, but the FF quasi-mode can interact via higher-order modes, thereby limiting the amount of frequency doubled power through Maker-like interference. Moreover, due to the particular geometry and in contrast to the collinear guided-wave case, the overlap integral with the TE_0 at ω is an increasing function of the modal order at 2ω, as displayed in the inset of Fig. 4. In any case, the EFDBPM clearly provides a more accurate estimate of the up-converted energy at the output.
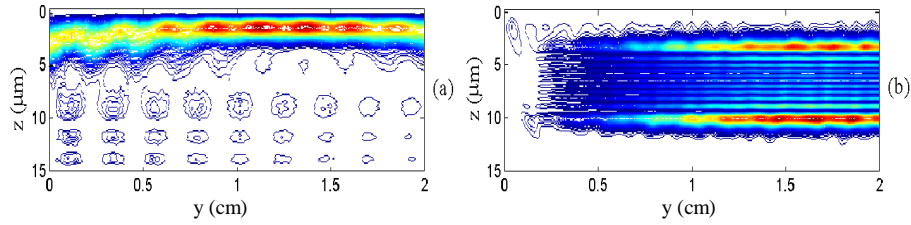
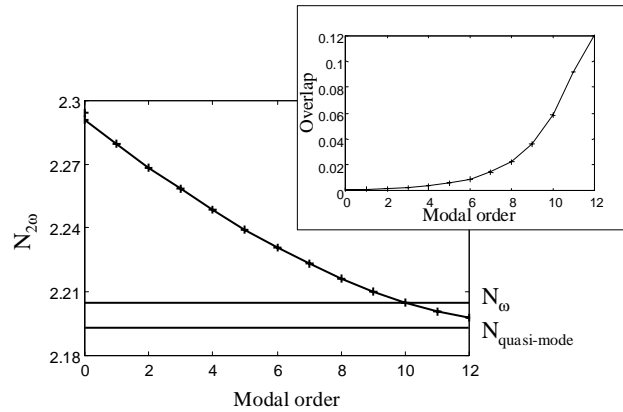Fig. 3. Contour maps of (a) FF and (b) SH intensity versus z and y for a Gaussian input at 10W/μm in a sample at temperature 25°C.

Fig. 4. Phase-matching diagram at 25°C versus modal order *m* at SH. The horizontal lines refer to the FF modes, TE_0 and leaky (or quasi-mode), respectively. The inset shows the corresponding TM_m-TE_0 overlap integral.

The conversion process can be enhanced by exciting only one FF mode, launching an input beam with transverse profile mapping the TE_0 mode. In this case, at an optimum temperature of 85°C corresponding to phase-matching, the SH grows monotonically along y largely depleting the fundamental, as visible in Fig. 5.

Using this optimum input profile, by a transverse integration in y=L we computed SHG conversion versus input FF power (in W/μm). The results are shown in Fig. 6 for two different sample lengths and temperatures. Due to the nature of the interaction and the substantial pump depletion, the conversion efficiency is sub-linear with both FF excitation and square of the propagation distance. For L=2cm it reaches 90% at 10W/μm, with a maximum normalized value of 14% μm/W cm (Fig. 6b, solid line). The temperature dependence, taken into account at each wavelength and polarization [12], is rather weak. This is clearly visible in Fig. 7, where the SHG efficiency is graphed versus temperature for two different input powers and sample lengths.
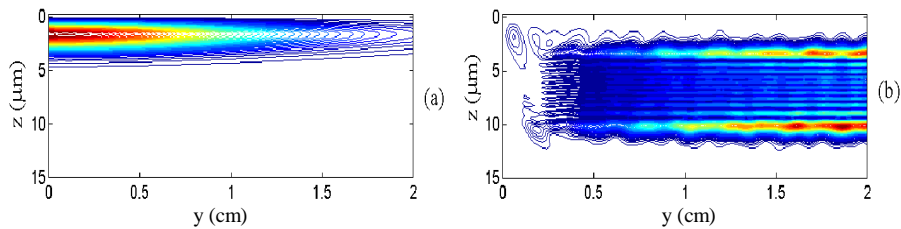

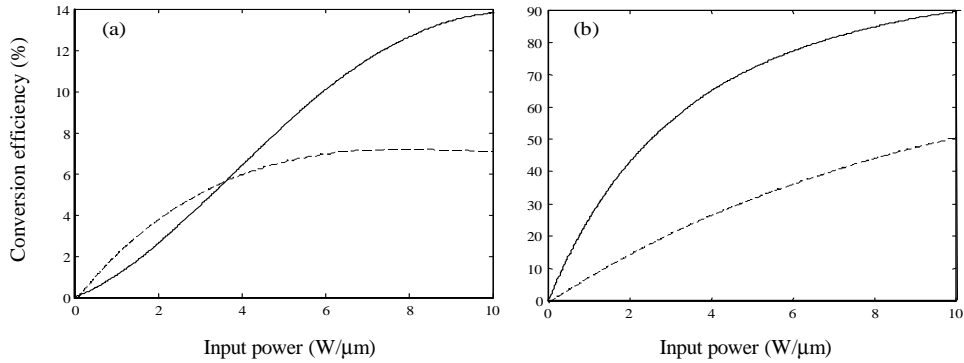Fig. 5. Contour maps of (a) FF and (b) SH intensity versus z and y for a TE_0 input at 10W/μm.

Fig. 6. Conversion efficiency versus input FF power (TE$_0$ excitation) at (a) 25 and (b) 85°C, for samples 1cm (dashed line) and 2cm (solid line) in length.
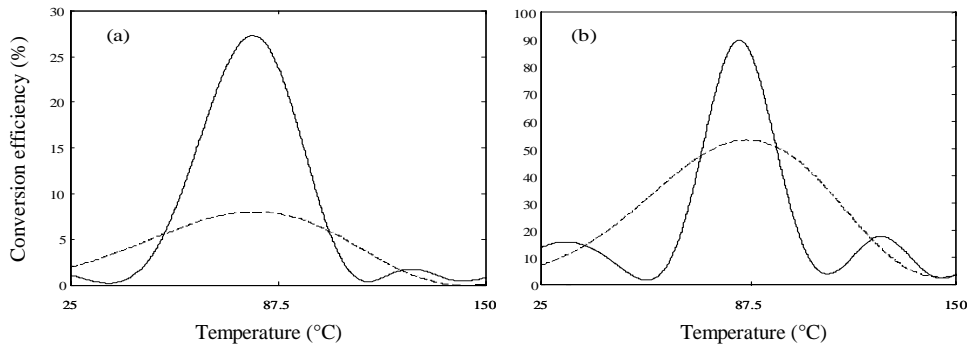

Fig. 7. Conversion efficiency versus temperature (TE$_0$ excitation) at input powers of (a) 1W/μm and (b) 10W/μm, for samples 1cm (dashed line) and 2cm (solid line) in length.

4. Conclusions

The major drawbacks of Cerenkov and temperature-tuned SHG, i. e. conical emission and critical thickness in PE waveguides [13-14] or critical temperature/modal tuning in Ti:in-diffused channels [15], respectively, can be eliminated in propagation-uniform Reverse Proton Exchanged guides in z-cut Lithium Niobate. The conversion efficiencies, numerically estimated using a propagator based on a robust PDE model, are as high as 90% at a fundamental wavelength of 1.32μm in 2cm-long planar guides optimally excited at 10W/μm. Such values compare well to the best results reported to date in non-periodically-poled LN (i. e., non quasi-phase-matched) waveguides, both in Cerenkov [16-17] and guided-wave interactions [15, 18].

RPE waveguides appear to be promising candidates for robust and low temperature frequency doubling, with the unique advantages of SH confinement, weak temperature sensitivity, polarization selection and physical separation of the harmonics at the output. We are currently investigating channel waveguides for bidimensional confinement and longitudinally tapered transverse profiles for improved coupling/handling of the up-converted output distribution.

Acknowledgements